Acta Materialia 246 (2023) 118700

Contents lists available at ScienceDirect

Acta Materialia

journal homepage: www.elsevier.com/locate/actamat

Full length article

Effects of size ratio on particle packing in binary glasses

Huijun Zhang [a,*], Chengjie Luo [b], Zhongyu Zheng [c,*], Yilong Han [d,*]

[a] State Key Laboratory for Mechanical Behaviour of Materials, Shaanxi International Research Center for Soft Matter, School of Materials Science and Engineering, Xi'an Jiaotong University, 710049, Xi'an, China
[b] Soft Matter and Biological Physics, Department of Applied Physics, Eindhoven University of Technology, Eindhoven, The Netherlands
[c] Institute of Mechanics, Chinese Academy of Sciences, School of Engineering Science, University of Chinese Academy of Sciences, Beijing, China
[d] Department of Physics, Hong Kong University of Science and Technology, Clear Water Bay, Hong Kong Special Administrative Region of China

ARTICLE INFO

Keywords:
Metallic glass
Binary hard-sphere glass
Amorphous structure
Non-cubic scaling law

ABSTRACT

Mixtures of binary spheres represent prototypes of amorphous solids and can model metallic, granular, and colloidal glasses. However, the effects of the size ratio λ on amorphous structures are not well understood. Here, we revisit the controversial noncubic scaling law and the local sphere packing by systematically changing λ. Our simulations clarify the existence and mechanism of the noncubic scaling law for mean atomic volume, $v_a \propto q_1^{-d}$, where q_1 is the position of the first diffraction peak and d is a constant less than the space dimension D. We find that the scaling law holds at each λ in binary hard-sphere glasses and metallic glasses, but the exponent satisfies a universal power law, $d \sim (\lambda - \lambda_c)^{-\gamma}$, instead of being a constant. The decreasing trend of $d(\lambda)$, the abnormal $d > D$ and the divergence of d when λ approaches 1 are theoretically explained. Moreover, d begins to fluctuate at $\lambda < 1.2$, indicating less stable glasses. Large and small spheres are better dispersed with more disordered structures at $\lambda > 1.2$. At $\lambda = 1.2$, various structural parameters change, and the number of icosahedral packing reaches the maximum. The results cast light and pose new challenges on amorphous structures of binary glasses.

1. Introduction

Glasses, i.e. amorphous solids, are usually produced by cooling [1] or densifying [2] liquids when crystallization is precluded. The mixing of different-sized spheres can effectively frustrate crystallization, and this approach is often used in glass productions [3–6]. Mixtures of binary spheres are one of the simplest types of glasses, and can model many granular, colloidal and metallic glasses (MGs). Binary glassy systems in granular matters [7,8], colloids [9–12] and alloys [3,13–17] have been intensively studied. These studies have focused on the slow dynamics [9,10,18–21], locally favoured structures [13,22], and medium-range order [9,12] in the supercooled regime; jamming transitions close to the high density limit [2,23]; and glass-forming ability [3,14,15,17]. However, the effects of the size ratio λ and the fraction of large spheres x on the glass structure have not been well understood. Here, we clarify the open problem about the noncubic scaling law, which has been mainly studied in MGs [24–28], by systematically changing the λ and x of binary hard-sphere glasses. Moreover, various structural parameters exhibit prominent changes at the special value of $\lambda = 1.2$.

In crystals, the first peak position q_1 of the structure factor $S(q)$ is inversely proportional to the lattice constant, that is, $q_1 \propto 1/a$. Therefore the mean volume per atom must satisfy $v_a \propto a^D \propto {q_1}^{-D}$ for a D-dimensional crystal. However, diffraction experiments and simulations showed that various MGs follow a noncubic scaling law:

$$v_a \propto q_1^{-d} \tag{1}$$

with a fractional exponent $d \simeq 2.5 < D = 3$ under compositional and pressure changes [24–26]. Recently, we found that this scaling law holds for glasses composed of hard and soft particles under pressure changes at fixed composition, whereas exponent d varies in two dimensions [29]. Whether Eq. (1) with $d \simeq 2.5$ generally holds in three-dimensional (3D) glasses remains controversial [26–28]. $S(q_1)$ contains structural information spanning broad length scales in real space. Therefore, the scaling law concerning q_1 in a reciprocal space is difficult to connect to certain structural changes in real space. The anomalous scaling law with $d < D$ has been attributed to fractal packing at the atomic level [25] or at the medium range [24]. However, further studies questioned if the noncubic scaling law can be attributed to the fractal structure [28,30,31]. Thus, the mechanism of noncubic scaling law remains elusive, and which factor affects the scaling law remains unclear. Here, we clarify that this scaling law holds in binary MGs and hard-sphere glasses under compositional changes at fixed

* Corresponding authors.
E-mail addresses: huijun@xjtu.edu.cn (H. Zhang), zzy@imech.ac.cn (Z. Zheng), yilong@ust.hk (Y. Han).

https://doi.org/10.1016/j.actamat.2023.118700
Received 22 September 2022; Received in revised form 5 January 2023; Accepted 10 January 2023
Available online 14 January 2023

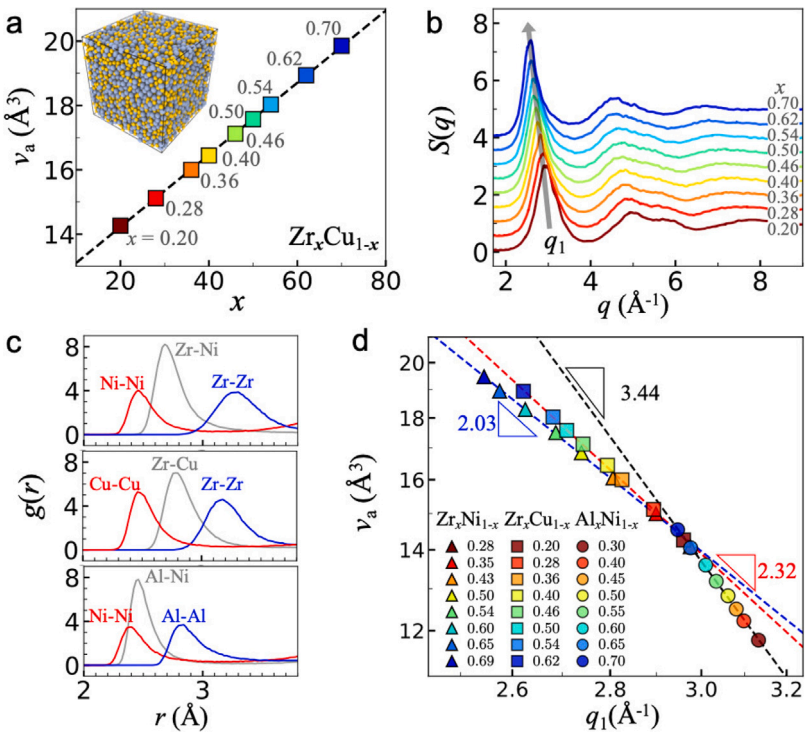

Fig. 1. Noncubic scaling laws in MGs under composition change. (a) v_a increases linearly with the fraction of Zr content in Zr_xCu_{1-x} MGs. Inset: $Zr_{0.5}Cu_{0.5}$ at 300 K and 0 Pa. Blue and yellow spheres denote Zr and Cu atoms, respectively. (b) Structure factor $S(q)$ at different compositions. The arrow shows the shift in q_1. (c) Measured partial radial distribution functions of the first-neighbour shell for $Zr_{0.5}Ni_{0.5}$, $Zr_{0.5}Cu_{0.5}$, and $Al_{0.5}Ni_{0.5}$. (d) Zr–Ni (triangles), Zr–Cu (squares) and Al–Ni (circles) MGs exhibit $v_a \propto q_1^{-d}$ (dashed lines in the log–log plot) with d = 2.03, 2.32, and 3.44, respectively. The errors are smaller than the symbols. (For interpretation of the references to colour in this figure legend, the reader is referred to the web version of this article.)

pressure, but breaks down when both pressure and composition change; Instead of a constant, the d of the scaling law varies with λ following a power law.

The measured scaling laws are compared with those for MGs in previous experiments [24,32,33] and simulations [28]. The results are in contrast with two previously held beliefs: (1) $d < D$ based on real-space fractal mechanisms, and (2) a general $d \simeq 2.5$ without λ dependence. We further observe various structure changes at $\lambda = 1.2$, which can partly explain the observed stability change.

2. Glass models

We perform molecular dynamics simulations [34] for MGs and event-driven molecular dynamics simulations [35] for hard-sphere glasses (see Supplementary for the details). Each glass sample contains N = 10,000 binary spheres in a cubic box under periodic boundary conditions. $\lambda = \sigma_A/\sigma_B > 1$, where σ is the diameter of the large (A) or small (B) spheres.

2.1. Metallic glass

Simulations for metallic glasses (MGs) are conducted using Large-scale Atomic/Molecular Massively Parallel Simulator (LAMMPS) [34] with the embedded-atom method (EAM) potentials [36–38]. The standard potential files are downloaded from https://www.ctcms.nist.gov/potentials/system/. The complicate many-body attractive EAM potentials are well tuned to fit a large set of atomic configurations, cohesive energies, atomic forces and stress tensors derived from ab initio calculations [36–38], and have been widely used in recent studies of MGs [15,17,25,28,39–45]. The Fast Inertial Relaxation Engine algorithm [46] is used to minimize the energy of the system and prevent particle overlap. Samples are first melted and relaxed at 2,000 K for 10 ns with a time step of 1 fs in an NPT (constant particle number N, pressure P, and temperature T) ensemble. The melts are then cooled to 300 K at 0 Pa at a fast-cooling rate of 10^{12} K/s to prevent crystallization. Such high cooling rate is sufficient to produce Al–Ni glasses as reported in Refs. [17,28], although Al–Ni is a poor glass former [15]. The resulting sample is relaxed further for 5 ns and 1,000 snapshots are extracted from the last 1 ns for structural analysis.

2.2. Hard-sphere glass

The hard-sphere potential is defined as

$$U(r) = \begin{cases} \infty & \text{for} \quad r \le \sigma_{ij} \\ 0 & \text{for} \quad r > \sigma_{ij}, \end{cases} \tag{2}$$

where r is the particle separation, σ_{ij} is the sum of the particle radii. The diameter of small (B) spheres $\sigma_{BB} = \sigma$ serves as the length unit, and the diameter of large (A) spheres is $\sigma_{AA} = \lambda\sigma$. $\sigma_{AB} = (\sigma_A + \sigma_B)/2$ is the interaction distance between large and small spheres. The phase behaviours of hard-sphere systems are determined by their volume fraction (i.e. density) rather than by the temperature. The volume fraction of A_xB_{1-x} is calculated using

$$\phi = \frac{N}{V}\frac{\pi\sigma^3}{6}(x\lambda^3 + 1 - x), \tag{3}$$

where V is the volume of the simulation box.

All results are averaged over ten samples for MGs and over five samples for hard-sphere glasses to give sufficient statistics. Note that all of the samples remain disordered glasses because they comprise of less than 1% crystalline particles according to polyhedral template matching method [47].

3. Results

We simulate typical MGs including Zr–Ni, Zr–Cu, Al–Ni, Zr–Cu–Al, and Zr–Cu–Ag alloys with different composition x. Fig. 1a shows that v_a

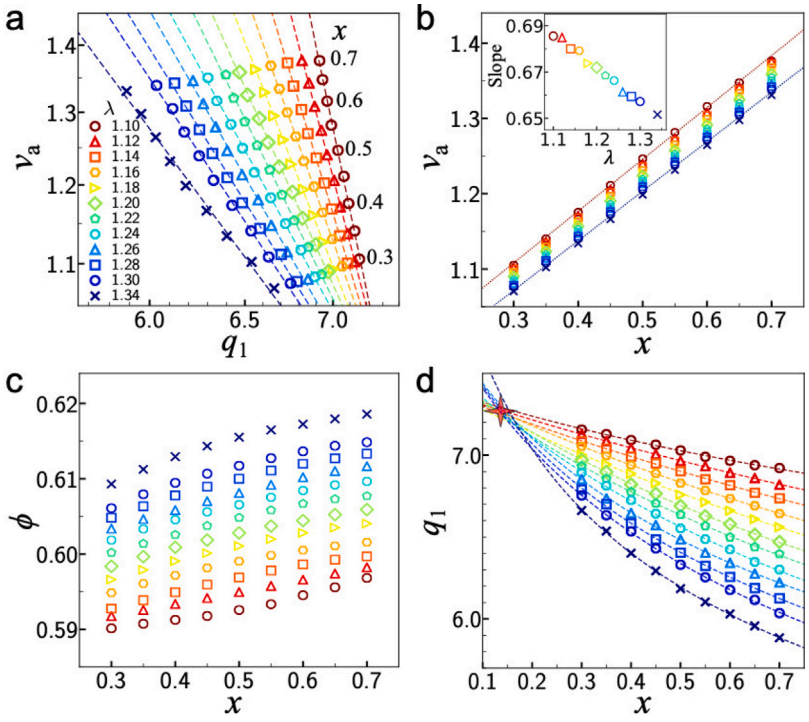

Fig. 2. Noncubic scaling laws in hard-sphere glasses. (a) Changing x from 0.3 to 0.7 at a fixed λ (symbol) gives $v_a \propto q_1^{-d}$ (dashed lines in the log–log plot). (b) Linear $v_a(x)$ at each λ. Inset: Slopes of the linear $v_a(x)$. (c) Volume fraction ϕ increases with x and is greater than the glass transition point $\phi_g \approx 0.585$ for hard-sphere systems [1,11]. (d) $q_1(x)$ at different λ values fitted with $q_1 \sim (c+x)^{-1/d}$ (dashed curves) intersect at $x \approx 0.13$ (red star).

of Zr_xCu_{1-x} increases linearly with x, indicating the linear additivity of the volumes of Zr and Cu which is common in MGs [32,33]. In addition, the higher number of large Zr atoms increases the mean interatomic separation in real space, which reduces the first peak position q_1 of $S(q)$ in the reciprocal space (Fig. 1b). Here, the structure factor: $S(q) = \langle \sum_{j=1}^{N} e^{i\mathbf{q}\cdot\mathbf{r}_j} \sum_{k=1}^{N} e^{-i\mathbf{q}\cdot\mathbf{r}_k} \rangle / N$ is calculated from the particle's position $\mathbf{r}$. The value of q_1 is measured from the Lorentzian fit of the first peak of $S(q)$ [29].

3.1. Noncubic scaling laws in MGs

Three types of binary MGs at 300 K and 0 Pa are compared in Fig. 1. Zr–Ni, Zr–Cu, and Al–Ni MGs possess different λ as shown by their partial radial distribution functions in the first-neighbour shell in Fig. 1c. Each peak denotes the typical interatomic distance [15,17]. The atomic diameters measured from peak positions agree with the values in the previous simulations [15,17]. Their size ratios λ are therefore 1.32, 1.27 and 1.18, respectively.

Fig. 1d shows that $d = 3.44 > D$ for Al–Ni alloys. Such abnormal $d > D$ behaviour has only been reported in a simulation of Al–Ni MGs in the Supplementary material of Ref. [28], but it was interpreted as evidence for the breakdown of the universal scaling law. Fig. 1d shows that the composition-induced noncubic scaling law holds well but has different exponents $d = 2.03$, 2.32, 3.44 in Zr–Ni, Zr–Cu, and Al–Ni MGs, respectively. By contrast, previous simulations and experiments fitted the mixed data of various MGs with different x, P or λ [24,26,28]; thus, they either cannot be well fitted with a single scaling law [28] or the fitted exponents are slightly inconsistent. Consequently, the validity of the scaling law with a universal $d \simeq 2.5$ is controversial. Here we find that d is not a universal constant and depends on λ (Fig. 1d). The above results represent only three λ values in a narrow range and are therefore not sufficient to reveal how size ratio affects the scaling law. We next study the effect of λ using binary hard-sphere glasses whose λ can be continuously tuned in a broad range.

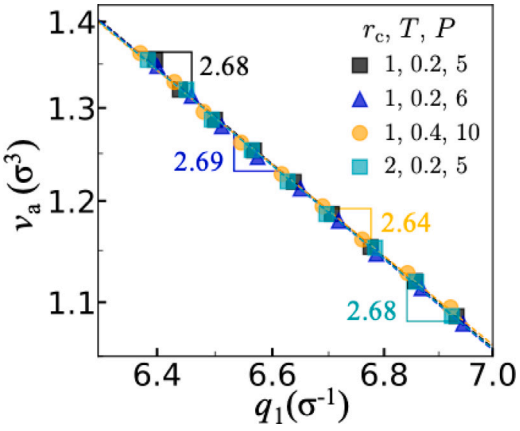

Fig. 3. Composition-induced noncubic scaling law is independent of conditions at a fixed λ. The log–log plots of $v_a(q_1)$ for hard-sphere glasses with $\lambda = 1.22$ at different compression rates (r_c), T, and P follow almost the same scaling law (dashed lines).

3.2. Noncubic scaling laws in hard-sphere glasses

Composition-induced scaling law has not been explored in hard-sphere glasses. We prepare the hard-sphere glasses by compressing liquids to a constant pressure $P = 5.5$ (Supplementary Fig. S1a). Systems under this pressure are dense enough to be in the glass regime with volume fractions $\phi > 0.585$ [1]. In Fig. 2a, hard-sphere glasses follow the scaling laws very well at $1.10 \le \lambda < 1.34$, but less well at $\lambda < 1.10$ and $\lambda > 1.34$, because of the crystallization and the separation of large and small spheres, respectively [48]. The noncubic scaling law [Eq. (1)] in hard-sphere glasses is robust at different (P,T) and compression rates (Fig. 3).

The linear $v_a(x)$ (Fig. 2b) reflects the simple additivity of volumes of binary hard spheres, similar to the behaviour of the MG in Fig. 1a. $v_a(q_1)$ and $v_a(x)$ in Fig. 2a and b yield $q_1 \sim [c(\lambda)+x]^{-1/d(\lambda)}$, where

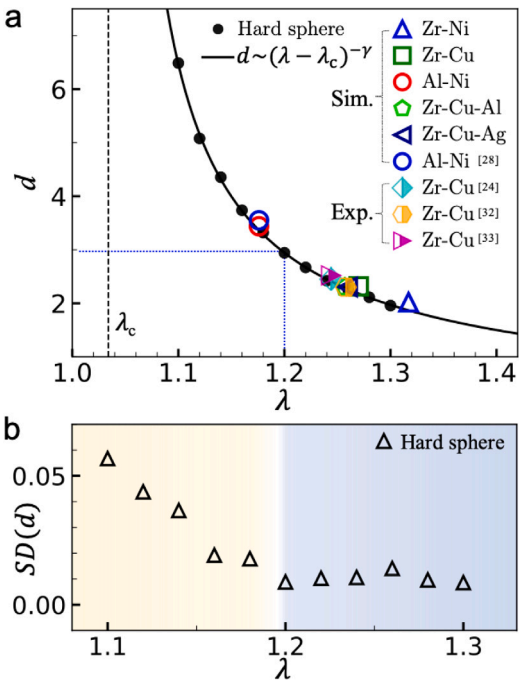

Fig. 4. Power law $d(\lambda)$. (a) All scaling exponents fall onto $d \sim (\lambda - \lambda_c)^{-\gamma}$ (black curve) with fitted $\lambda_c = 1.034 \pm 0.005$ (vertical line) and $\gamma = 0.853 \pm 0.038$. Coloured open symbols represent the results of MG simulations, and the half-filled symbols are extracted from the experimental literature [24,32,33] (Supplementary Fig. S3). (b) Standard deviations of d. (For interpretation of the references to colour in this figure legend, the reader is referred to the web version of this article.)

c is a constant for each λ. Such a functional form fits $q_1(x)$ well in Fig. 2d, and all fitted curves for different λ values intersect at $x \approx 0.13$, implying that the λ–induced size mismatch is indiscernible for q_1 at $x \leq 0.13$. Therefore, more than 13% large spheres are needed to produce the considerable structural mismatch for glass formation, which is consistent with the report that more than 11% Zr atoms are needed to form Zr–Cu MGs [3,49].

The linear $v_a(x)$ in Fig. 2b shows that the volume additivity is independent of λ, thus $v_a(x)$ contributes little to the λ dependence of the scaling law in Fig. 2a. Therefore, the λ dependence of the scaling law (Fig. 2a) is derived solely from the λ dependence of $q_1(x)$ in Fig. 2d. This finding can be qualitatively explained as follows: $q_1(x)$ obviously decreases with x, because the presence of more large spheres increases the mean real-space interparticle distance, which leads to the decrease in q_1 in the reciprocal space. Such an effect is more prominent at larger λ values, resulting in the steeper slope of $q_1(x)$ in Fig. 2d and the smaller d in Fig. 2a.

3.3. General power law for exponent d

The exponents d of the scaling laws, i.e., the slopes in Figs. 1d and 2a, vary with λ. Interestingly, they collapse into a power law:

$$d \propto (\lambda - \lambda_c)^{-\gamma}, \tag{4}$$

where $\gamma = 0.853$ and $\lambda_c = 1.034$ (Fig. 4a). This increasing trend in d indicates that when compositional change causes a finite change in v_a, q_1 changes little approaching $\lambda = 1.034$. This result is very close to Egami's prediction of the glass forming regime $\lambda_e > 1.04$ for binary-sphere model [50]. Note that the glasses are below the close-packing density, and the gaps between particles can slightly reduce Egami's threshold, making it closer to our fitted λ_c (see Supplementary S7).

The power law behaviour [Eq. (4)] in Fig. 4a remains robust under thermal fluctuations as shown in Supplementary Fig. S1b. The λ-dependent scaling law also holds for hard-sphere glasses at other (P, T) and compression rate (Fig. 3). v_a and q_1 slightly change concurrently under different compression rates, but d is barely affected (Fig. 3). Moreover, a quantitative prediction of Eq. (1) from the Ornstein–Zernike relation with the Percus–Yevick approximation [51,52] (see Supplementary S10 for the details) deviates from the simulation and experimental results (Fig. 4a and supplementary Fig. S8), indicating that the noncubic scaling law is indeed a non-trivial relation.

In Fig. 4a, $d > D$ when $\lambda < 1.2$, which is in accordance with our simulated value of $d = 3.44$ for Al–Ni MGs in Fig. 1d, whose $\lambda = 1.18$. Remarkably, the d values from our simulations in Fig. 1d and the available experimental results in the literature for MGs all follow this general power law precisely as shown in Fig. 4a. In addition, our simulations show that the noncubic scaling law also holds for ternary $Zr_xCu_{0.9-x}Al_{0.1}$ and $Zr_xCu_{0.9-x}Ag_{0.1}$ MGs, and that their d values agree well with the power law in Fig. 4a. The third type of atom (i.e., Al or Ag) has a fixed, low concentration; thus, the scaling law arises from changes in Zr and Cu concentrations. Here, λ is the ratio between the effective diameters of Zr and Cu atoms weighted by Al or Ag atoms (see Supplementary S6 for the details).

Our measured size ratios of the binary atoms perfectly agree with those in Refs. [15,17] using the same EAM potentials, but slightly larger than the experimental values [3,49,53]. Nevertheless, EAM potentials are one of the most accurate models for metallic glasses by now. Moreover, the noncubic scaling law is robust for experimental MG data and simulation data with the EAM potentials, indicating its robustness for different interaction potentials. Note that the noncubic scaling only holds for each λ under a fixed P at different x, or at a fixed x under different P. A single scaling law cannot well fit the data under different P and x, see Supplementary S8 and Fig. S5.

3.4. Theoretical proof of the divergence of d

As the fraction of large particle x increases in a series of MG samples under a constant pressure (e.g., Supplementary Fig. S9), the concurrent changes of $v_a(x)$ and $q_1(x)$ yield the noncubic scaling law of Eq. (1). According to Eq. (1),

$$d = -\frac{\mathrm{d}\ln v_a}{\mathrm{d}\ln q_1}. \tag{5}$$

The volume additivity in binary glasses under a constant pressure [32,33] leads to the linear relation $v_a = c_0 + c_1 x$, where $c_{0,1}$ are constant. Thus,

$$d = -\frac{\frac{\mathrm{d}\ln v_a}{\mathrm{d}x}}{\frac{\mathrm{d}\ln q_1}{\mathrm{d}x}} = -\frac{\frac{c_1}{v_a}}{\frac{\mathrm{d}q_1}{q_1\mathrm{d}x}} \simeq -\frac{c_1}{\frac{v_a \Delta q_1}{q_1 \Delta x}}. \tag{6}$$

Next, we show that the denominator can approach 0 so that d can be infinity. Replacing Δx fraction of small particles with large ones increases the mean interparticle distance and thus reduces q_1. q_1 is less affected by Δx when λ is small. When λ approaches 1, the small and large particles have almost the same size, and thus Δq_1 is infinitely small by replacing a fixed Δx fraction of particles. Therefore, d diverges as $\lambda \to 1$ since q_1 and v_a in the denominator of Eq. (6) are finite. As the intermediate steps of the above derivation, the linear $v_a(x)$ and the lower slope of $q_1(x)$ at small λ are confirmed in Figs. 1a and 2d, respectively. The above analysis only gives the lower bound of λ for the divergent d, thus in accordance with the fitted $\lambda = 1.03$ in Fig. 4a. It is also possible that the fitting Eq. (4) does not work well when λ is very close to 1.03.

3.5. Effect of λ on glass stability

We find that d is stable at $\lambda \geq 1.2$ (i.e., $d < 3$ regime) and fluctuates strongly at $\lambda < 1.2$ (i.e., $d > 3$ regime), especially for small λ as shown in Fig. 4b. This result implies stronger structural fluctuations at $\lambda < 1.2$ (also shown in Supplementary Fig. S6), which can promote devitrification. Therefore, glasses with $\lambda < 1.2$ are less stable. This

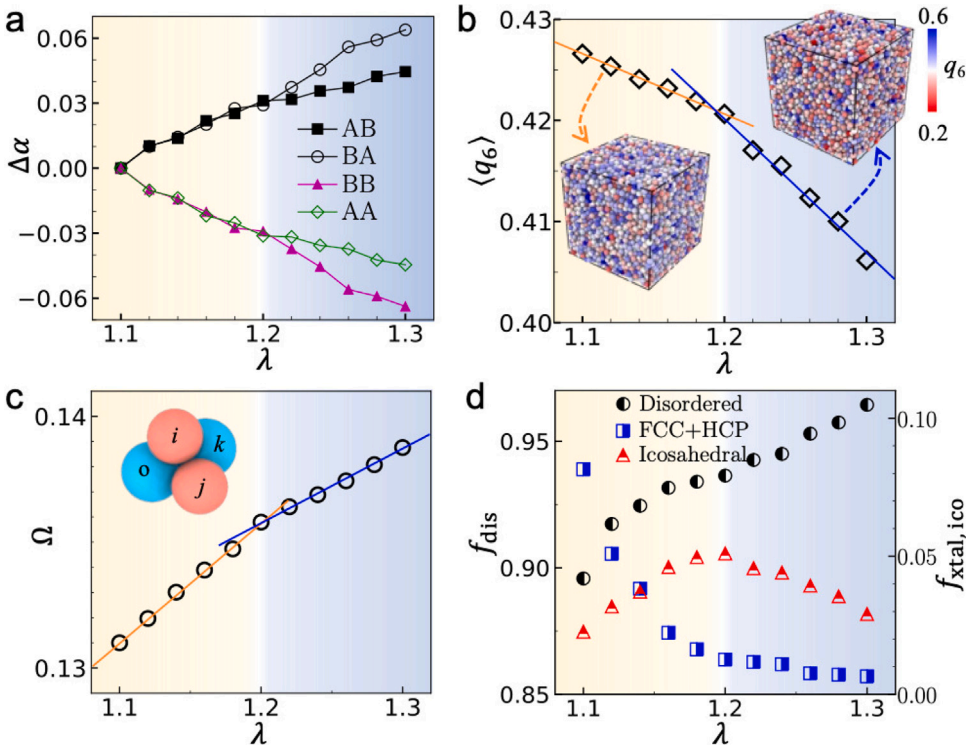

Fig. 5. Structural changes at $\lambda = 1.2$ for systems at $x = 0.5$ and $\phi = 0.59$. (a) Particles' aggregation propensity $\Delta\alpha = \alpha(\lambda) - \alpha(1.1)$ for AB (B-type particles around A-type particles), BA, AA, and BB bonds, respectively. (b) $\langle q_6 \rangle$ decreases with λ. Insets: The glass with $\lambda = 1.28$ contains more disordered (i.e., low q_6) particles than that with $\lambda = 1.12$. (c) Average local packing capability parameter Ω. Inset: A local tetrahedron composed of two large (blue) and two small (red) spheres. (d) Fractions of disordered, crystalline (FCC and HCP), and icosahedral structures. (For interpretation of the references to colour in this figure legend, the reader is referred to the web version of this article.)

finding agrees with the anomalously slower crystal growth and better glass-forming ability of Zr–Cu than those of Al–Ni in Ref. [15] because $\lambda > 1.2$ for Zr–Cu and $\lambda < 1.2$ for Al–Ni. Besides the structure fluctuation, interatomic potential also takes significant role on the glass forming ability [15]. The Al–Ni peak position deviates from the average of the Ni–Ni and Al–Al distances in Fig. 1c, indicating a strong Al–Ni interaction and non-additivity in particle size [15]. This effect can reduce the glass forming ability [15].

3.6. Effects of λ on glass structure

The systematic adjustment of λ in hard-sphere glasses enables the measurement of its effects on the noncubic scaling law and other structural properties, such as neighbouring pairs [54], local crystalline order [55], local packing capability [21], and icosahedral packing [47].

3.6.1. Short-range order

For binary systems, the neighbouring pair or chemical short-range order is characterized by the Warren–Cowley parameter [54],

$$\alpha_{\rm AB} = 1 - \frac{Z_{\rm AB}}{x_{\rm B} Z_{\rm A}}, \tag{7}$$

where $Z_{\rm A}$ is the coordination number of A-type particle; $Z_{\rm AB}$ is the number of B-type particles neighbouring around A, and $x_{\rm B}$ is the fraction of B-type particles. $\alpha_{\rm AB} = 0, > 0$ and < 0 correspond to random mixture, favoured and unfavoured AB bonds, respectively. $\Delta\alpha \equiv \alpha(\lambda) - \alpha(\lambda = 1.1)$ in Fig. 5a shows that $\Delta\alpha_{\rm AB,BA} > 0$ and $\Delta\alpha_{\rm AA,BB} < 0$, indicating that the differently sized particles have a high affinity than the same sized particles. This trend increases (i.e., particles are better mixed) as λ increases. $\Delta\alpha_{\rm AB}$ and $\Delta\alpha_{\rm BA}$ bifurcate at $\lambda \geq 1.2$ in Fig. 5a, implying that a small particle surrounded by large ones occurs more often than a large particle surrounded by small ones at $\lambda > 1.2$. Such tendency of aggregation between large particles becomes more prominent at $\lambda > 1.2$ (see Supplementary Fig. S7), which enhances the stability as shown in Fig. 4b.

3.6.2. Bond-orientational order

The modified bond-orientational order parameter q_6 [5,55] is applied to characterize the local crystalline order of each particle i,

$$q_6 = \sqrt{\frac{4\pi}{2l+1} \sum_{m=-l}^{l} \left| \sum_{j=1}^{n} \frac{A_j}{A} Y_{lm}(\theta_{ij}, \phi_{ij}) \right|^2} \tag{8}$$

θ_{ij} and ϕ_{ij} are the spherical angles of the vector from particle i to its jth nearest neighbour. A_j is the area of the Voronoi facet to the jth neighbour and A is the total surface area of the Voronoi cell. Y_{lm} is a spherical harmonic function of degree l and order m. Thus, each neighbour of particle i is properly weighted by the corresponding facet of the Voronoi cell in q_6 [55]. A lower value of q_6 represents a more disordered structure around particle i [56]. Fig. 5b shows that the averaged q_6 decreases with λ and exhibits a slope change at $\lambda = 1.2$. The high $\langle q_6 \rangle$ at $\lambda < 1.2$ is in accordance with the faster crystal growth observed in Al–Ni alloy [15], whose $\lambda < 1.2$, which corresponds to the large structural fluctuation at $d > 3.0$ in Fig. 4b.

3.6.3. Local packing capability

The basic 3D building block is a tetrahedron packed by four spheres which is closely related to the dynamics of hard-sphere glass [6]. Tong et al. recently proposed the local packing capability of particle o, Ω_o, to measures its deviation from the reference close-packing tetrahedra [21]:

$$\Omega_o = \frac{1}{N_o^{\rm tetra}} \sum_{\langle oijk \rangle} \omega_{\langle oijk \rangle}, \tag{9}$$

with

$$\omega_{\langle oijk \rangle} = \frac{\sum_{\langle ab \rangle} |r_{ab} - \sigma_{ab}|}{\sum_{\langle ab \rangle} \sigma_{ab}}, \tag{10}$$

where $N_o^{\rm tetra}$ is the total number of tetrahedra surrounding particle o, and the summation runs over all these tetrahedra. $\omega_{\langle oijk \rangle}$ measures

the irregularity of the tetrahedron $\langle oijk\rangle$ formed by particles o, i, j and k, with $\langle ab\rangle$ running over its six edges; r_{ab} is the measured distance between particles a and b; and σ_{ab} is the ideal distance between a and b in the reference tetrahedron. Ω can detect disorderness in an order-agnostic manner especially in non-monodispersed systems without a prior knowledge of the preferred local structure or symmetry. The larger Ω values indicate stronger deviations from sterically favoured tetrahedra and hence higher disorder. Ω is effective in revealing the dynamic slowing down of binary hard-sphere fluids [21]. Here we use it to characterize the glass structure at different size ratios. In Fig. 5c, the averaged $\Omega(\lambda)$ increases, indicating a higher degree of disorder at a larger size ratio. $\Omega(\lambda)$ exhibits two linear regimes with a slope change at $\lambda = 1.2$. These results indicate that better dispersed large and small spheres at large λ distort the locally favoured packing from the reference tetrahedron (Fig. 5c).

3.6.4. Disordered, crystalline and icosahedral structures

Icosahedral, face-centred cubic (FCC), and hexagonal close-packed (HCP) structures are the equally densest packings for a sphere and its 12 monodispersed first-layer neighbours [13,57,58]. An icosahedron of 13 spheres interacting through a Lennard–Jones potential has a lower energy than structure of FCC or HCP, and it is therefore common in liquids [57]. The five-fold symmetry of icosahedra is incompatible with the crystalline order; thus, glasses can easily form. For example, icosahedra have been observed in various binary glasses [13,22,59]. Each particle is classified as disordered, crystalline (i.e., FCC and HCP), or icosahedral by polyhedral template matching method [47]. We set the cutoff of a structure deviation [47] as 0.15 to make the crystalline and icosahedral structures prominent. As λ increases, the fraction of disordered particles increases and the fraction of crystalline particles decreases in Fig. 5d. Interestingly, the fraction of icosahedral structure peaks at $\lambda = 1.2$ as shown in Fig. 5d. Icosahedral structures play remarkable roles in glassy behaviours for binary Lennard–Jones system [60], but exhibit negligible effects in colloidal glasses [61]. Our finding reconciles this discrepancy as spheres are bidispersed with $\lambda = 1.2$ in Ref. [60] and polydispersed in Ref. [61].

4. Summary and conclusions

We demonstrate that composition-induced noncubic scaling laws hold well in binary MGs and hard-sphere glasses by systematically changing λ of binary-sphere systems. Surprisingly, the exponent d can be larger than the space dimension 3, which rules out the mechanism of the noncubic scaling law based on real-space fractal structures. This is consistent with Refs. [28,30,31] which also suggested that the noncubic scaling law does not arise from real-space fractal structures. In addition, we find that d obeys the power law in Eq. (4) instead of being a constant of 2.5 [25,26] as previous works assumed. The decreasing $d(\lambda)$ in Fig. 4a arises from the linear $v_a(x)$ and the steeper slope of $q_1(x)$ for larger λ. This mechanism sets no upper limit, such as D, for d. We theoretically show that d should diverge when $\lambda \to 1$ in binary glasses with different mixing ratios under a constant pressure. Note that the exponent $d > D = 3$ in small-λ systems (Fig. 4a) is measured in the reciprocal space based on all particles, which does not conflict with the real-space fractals with $d < 3$ formed by a certain subset of particles (e.g., particles with icosahedral neighbours) observed in MGs [25,31,62,63]. The fractal formed by a subset of particles is measured from the structure of a single MG sample [25,31,62,63], while the noncubic scaling law of Eq. (1) is about the changing rate of $v_a(x)$ and $q_1(x)$ in a series of samples with different x, instead of about certain structure in a single sample. The exponent d depends on the relative change between $v_a(x)$ and $q_1(x)$ (Fig. 2a,b,d) and is not relevant to space dimension. We suggest to conduct an experimental search for the previously unexpected $d > D$ by using Al–Ni MGs in a broad composition range because their λ is small enough. The divergence of d has not been observed experimentally or numerically before because the currently available experimental and numerical data about changing mixing ratio in binary glasses are obtained from systems with $\lambda > 1.15$ as we summarized in Fig. 4a. Cu and Ni atoms have similar sizes in alloys, thus Cu–Ni MGs should have a large d. However, Cu–Ni systems have a very weak glass forming ability and can easily crystallize [3] under the currently available cooling rate, thus their d value has not been measured. This is consistent with the observations that the amorphous structure becomes less stable when $\lambda < 1.2$.

Besides the noncubic scaling law, we find that small particles are better dispersed (small $\Delta\alpha_{BB}$ in Fig. 5a) at $\lambda > 1.2$, and the associated structure is more disordered (Fig. 5a–d) with a higher stability (Fig. 4b). We observe a special value of $\lambda = 1.2$ for binary hard-sphere glasses, which has not been reported before. It is special in the following aspects: (1) $d = D = 3$ at $\lambda = 1.2$, indicating that the composition and pressure have the same effect on the noncubic scaling law (Fig. 4a; Supplementary S8 and Fig. S5). (2) The structural parameters in Fig. 5a–d exhibit slope changes. (3) The number of icosahedral packing peaks at $\lambda = 1.2$ when $x \geq 0.5$ (see Supplementary Fig. S10), which reconciles the observations that icosahedral structures are important in some glasses [60] but not in others [6,61].

Declaration of competing interest

The authors declare that they have no known competing financial interests or personal relationships that could have appeared to influence the work reported in this paper.

Acknowledgements

This work was supported by the Fundamental Research Funds for Central Universities, China (grant No. xxj032021001), the Key R&D Project of Shaanxi Province, China (grant No. 2022GY-400), the National Natural Science Foundation of China (grant No. 12274336), the Hong Kong Research Grants Council (grant No. CRF-C6016-20G, C6021-19EF), the Guangdong Basic and Applied Basic Research Foundation, China (grant No. 2020B1515120067), the National Key R&D Program of China (grant No. 2022YFF0503500), and the China Manned Space Engineering Program.

Appendix A. Supplementary data

Supplementary material related to this article can be found online at https://doi.org/10.1016/j.actamat.2023.118700.

References

[1] L. Berthier, G. Biroli, Theoretical perspective on the glass transition and amorphous materials, Rev. Modern Phys. 83 (2011) 587.
[2] G. Parisi, F. Zamponi, Mean-field theory of hard sphere glasses and jamming, Rev. Modern Phys. 82 (2010) 789.
[3] T. Egami, Y. Waseda, Atomic size effect on the formability of metallic glasses, J. Non-Cryst. Solids 64 (1984) 113–134.
[4] L. Wang, N. Xu, W. Wang, P. Guan, Revealing the link between structural relaxation and dynamic heterogeneity in glass-forming liquids, Phys. Rev. Lett. 120 (2018) 125502.
[5] H. Zhang, Y. Han, Compression-induced polycrystal-glass transition in binary crystals, Phys. Rev. X 8 (2018) 041023.
[6] S. Marín-Aguilar, H.H. Wensink, G. Foffi, F. Smallenburg, Tetrahedrality dictates dynamics in hard sphere mixtures, Phys. Rev. Lett. 124 (2020) 208005.
[7] A. Seguin, O. Dauchot, Experimental evidence of the gardner phase in a granular glass, Phys. Rev. Lett. 117 (2016) 228001.
[8] L. Zhang, J. Zheng, Y. Wang, L. Zhang, Z. Jin, L. Hong, Y. Wang, J. Zhang, Experimental studies of vibrational modes in a two-dimensional amorphous solid, Nature Commun. 8 (2017) 1–9.
[9] H. Tanaka, T. Kawasaki, H. Shintani, K. Watanabe, Critical-like behaviour of glass-forming liquids, Nature Mater. 9 (2010) 324–331.
[10] K.H. Nagamanasa, S. Gokhale, A. Sood, R. Ganapathy, Direct measurements of growing amorphous order and non-monotonic dynamic correlations in a colloidal glass-former, Nat. Phys. 11 (2015) 403–408.

[11] G.L. Hunter, E.R. Weeks, The physics of the colloidal glass transition, Rep. Progr. Phys. 75 (2012) 066501.
[12] I. Tah, S. Sengupta, S. Sastry, C. Dasgupta, S. Karmakar, Glass transition in supercooled liquids with medium-range crystalline order, Phys. Rev. Lett. 121 (2018) 085703.
[13] H. Sheng, W. Luo, F. Alamgir, J. Bai, E. Ma, Atomic packing and short-to-medium-range order in metallic glasses, Nature 439 (2006) 419.
[14] Y. Li, Q. Guo, J. Kalb, C. Thompson, Matching glass-forming ability with the density of the amorphous phase, Science 322 (2008) 1816–1819.
[15] C. Tang, P. Harrowell, Anomalously slow crystal growth of the glass-forming alloy cuzr, Nature Mater. 12 (2013) 507.
[16] Y. Liu, T. Fujita, D. Aji, M. Matsuura, M. Chen, Structural origins of johari-goldstein relaxation in a metallic glass, Nature Commun. 5 (2014) 1–7.
[17] Z. Wu, M. Li, W. Wang, K. Liu, Hidden topological order and its correlation with glass-forming ability in metallic glasses, Nature Commun. 6 (2015) 6035.
[18] W. Kob, C. Donati, S.J. Plimpton, P.H. Poole, S.C. Glotzer, Dynamical heterogeneities in a supercooled lennard-jones liquid, Phys. Rev. Lett. 79 (1997) 2827.
[19] G. Biroli, S. Karmakar, I. Procaccia, Comparison of static length scales characterizing the glass transition, Phys. Rev. Lett. 111 (2013) 165701.
[20] R. Miyazaki, T. Kawasaki, K. Miyazaki, Cluster glass transition of ultrasoft-potential fluids at high density, Phys. Rev. Lett. 117 (2016) 165701.
[21] H. Tong, H. Tanaka, Revealing hidden structural order controlling both fast and slow glassy dynamics in supercooled liquids, Phys. Rev. X 8 (2018) 011041.
[22] C.P. Royall, S.R. Williams, The role of local structure in dynamical arrest, Phys. Rep. 560 (2015) 1–75.
[23] I. Biazzo, F. Caltagirone, G. Parisi, F. Zamponi, Theory of amorphous packings of binary mixtures of hard spheres, Phys. Rev. Lett. 102 (2009) 195701.
[24] D. Ma, A.D. Stoica, X.-L. Wang, Power-law scaling and fractal nature of medium-range order in metallic glasses, Nature Mater. 8 (2009) 30–34.
[25] D.Z. Chen, C.Y. Shi, Q. An, Q. Zeng, W.L. Mao, W.A. Goddard, J.R. Greer, Fractal atomic-level percolation in metallic glasses, Science 349 (2015) 1306–1310.
[26] Q. Zeng, Y. Lin, Y. Liu, Z. Zeng, C.Y. Shi, B. Zhang, H. Lou, S.V. Sinogeikin, Y. Kono, C. Kenney-Benson, C. Park, W. Yang, W. Wang, H. Sheng, H. kwang Mao, W.L. Mao, General 2.5 power law of metallic glasses, Proc. Natl. Acad. Sci. 113 (2016) 1714–1718.
[27] C. Xia, J. Li, B. Kou, Y.J. Wang, Origin of noncubic scaling law in disordered granular packing, Phys. Rev. Lett. 118 (2017) 238002.
[28] J. Ding, M. Asta, R.O. Ritchie, On the question of fractal packing structure in metallic glasses, Proc. Natl. Acad. Sci. 114 (2017) 8458.
[29] H. Zhang, K. Qiao, Y. Han, Power laws in pressure-induced structural change of glasses, Nature Commun. 11 (2020) 2005.
[30] P. Chirawatkul, A. Zeidler, P.S. Salmon, S. Takeda, Structure of eutectic liquids in the Au-Si, Au-Ge, and Ag-Ge binary systems by neutron diffraction, Phys. Rev. B 83 (2011) 014203.
[31] J. Feng, P. Chen, M. Li, Existence of fractal packing in metallic glasses: Molecular dynamics simulations of $Cu_{46}Zr_{54}$, Phys. Rev. B 98 (2018) 024201.
[32] Y. Calvayrac, J.P. Chevalier, M. Harmelin, A. Quivy, J. Bigot, On the stability and structure of Cu-Zr based glasses, Phil. Mag. B 48 (1983) 323–332.
[33] N. Mattern, A. Schöps, U. Kühn, J. Acker, O. Khvostikova, J. Eckert, Structural behavior of Cu_xZr_{100-x} metallic glass ($x = 35-70$), J. Non-Cryst. Solids 354 (2008) 1054–1060.
[34] S. Plimpton, Fast parallel algorithms for short-range molecular dynamics, J. Comput. Phys. 117 (1995) 1–19.
[35] M.N. Bannerman, R. Sargant, L. Lue, Dynamo: a free general event-driven molecular dynamics simulator, J. Comput. Chem. 32 (2011) 3329–3338.
[36] Y. Mishin, M.J. Mehl, P. D. A, Embedded-atom potential for B2-NiAl, Phys. Rev. B 65 (2002) 224114.
[37] M. Mendelev, M. Kramer, R. Ott, D. Sordelet, D. Yagodin, P. Popel, Development of suitable interatomic potentials for simulation of liquid and amorphous Cu–Zr alloys, Phil. Mag. 89 (2009) 967–987.
[38] M. Mendelev, M. Kramer, S. Hao, K. Ho, C. Wang, Development of interatomic potentials appropriate for simulation of liquid and glass properties of $NiZr_2$ alloy, Phil. Mag. 92 (2012) 4454–4469.
[39] P. Guan, M. Chen, T. Egami, Stress-temperature scaling for steady-state flow in metallic glasses, Phys. Rev. Lett. 104 (2010) 205701.
[40] Y. Cheng, E. Ma, Atomic-level structure and structure–property relationship in metallic glasses, Prog. Mater. Sci. 56 (2011) 379–473.
[41] T.C. Hufnagel, C.A. Schuh, M.L. Falk, Deformation of metallic glasses: Recent developments in theory, simulations, and experiments, Acta Mater. 109 (2016) 375–393.
[42] P. Zhang, J.J. Maldonis, M. Besser, M. Kramer, P.M. Voyles, Medium-range structure and glass forming ability in Zr–Cu–Al bulk metallic glasses, Acta Mater. 109 (2016) 103–114.
[43] P. Zhao, J. Li, J. Hwang, Y. Wang, Influence of nanoscale structural heterogeneity on shear banding in metallic glasses, Acta Mater. 134 (2017) 104–115.
[44] H.-B. Yu, R. Richert, R. Maaß, K. Samwer, Strain induced fragility transition in metallic glass, Nature Commun. 6 (2015) 1–6.
[45] B. Shang, W. Wang, A.L. Greer, P. Guan, Atomistic modelling of thermal-cycling rejuvenation in metallic glasses, Acta Mater. 213 (2021) 116952.
[46] E. Bitzek, P. Koskinen, F. Gähler, M. Moseler, P. Gumbsch, Structural relaxation made simple, Phys. Rev. Lett. 97 (2006) 170201.
[47] P.M. Larsen, S. Schmidt, J. Schiøtz, Robust structural identification via polyhedral template matching, Modelling Simul. Mater. Sci. Eng. 24 (2016) 055007.
[48] Y. Nie, J. Liu, J. Guo, N. Xu, Connecting glass-forming ability of binary mixtures of soft particles to equilibrium melting temperatures, Nature Commun. 11 (2020) 3198.
[49] K. Laws, D. Miracle, M. Ferry, A predictive structural model for bulk metallic glasses, Nature Commun. 6 (2015) 8123.
[50] T. Egami, Universal criterion for metallic glass formation, Mater. Sci. Eng. A 226 (1997) 261–267.
[51] J.L. Lebowitz, Exact solution of generalized Percus-Yevick equation for a mixture of hard spheres, Phys. Rev. 133 (1964) A895.
[52] R.J. Baxter, Ornstein–Zernike relation and Percus–Yevick approximation for fluid mixtures, J. Chem. Phys. 52 (1970) 4559–4562.
[53] D. Miracle, D. Louzguine-Luzgin, L. Louzguina-Luzgina, A. Inoue, An assessment of binary metallic glasses: correlations between structure, glass forming ability and stability, Int. Mater. Rev. 55 (2010) 218–256.
[54] B.E. Warren, X-Ray Diffraction, Dover Publications Inc, New York, 1990.
[55] W. Mickel, S.C. Kapfer, G.E. Schröder-Turk, K. Mecke, Shortcomings of the bond orientational order parameters for the analysis of disordered particulate matter, J. Chem. Phys. 138 (2013) 044501.
[56] H. Zhang, S. Peng, X. Zhou, X. Ju, Polymorphic crystals selected in the nucleation stage, Europhys. Lett. 107 (2014) 46002.
[57] F.C. Frank, Supercooling of liquids, Proc. R. Soc. Lond. Ser. A Math. Phys. Eng. Sci. 215 (1952) 43–46.
[58] V.N. Manoharan, Colloidal matter: Packing, geometry, and entropy, Science 349 (2015) 1253751.
[59] A. Hirata, P. Guan, T. Fujita, Y. Hirotsu, A. Inoue, A.R. Yavari, T. Sakurai, M. Chen, Direct observation of local atomic order in a metallic glass, Nature Mater. 10 (2011) 28.
[60] F. Turci, G. Tarjus, C.P. Royall, From glass formation to icosahedral ordering by curving three-dimensional space, Phys. Rev. Lett. 118 (2017) 215501.
[61] M. Leocmach, H. Tanaka, Roles of icosahedral and crystal-like order in the hard spheres glass transition, Nature Commun. 3 (2012) 974.
[62] M.H. Yang, J.H. Li, B.X. Liu, Fractal analysis on the cluster network in metallic liquid and glass, J. Alloys Compd. 757 (2018) 228–232.
[63] M. Kbirou, M. Mazroui, A. Hasnaoui, Atomic packing and fractal behavior of al-co metallic glasses, J. Alloys Compd. 735 (2018) 464–472.